Journal of the Physical Society of Japan **86**, 054401 (2017)
https://doi.org/10.7566/JPSJ.86.054401

Impact of Backscattering in Silicon Micro-ring Resonators on Photon Pair Generation

Jing Suo, Wei Zhang*, and Yidong Huang

Tsinghua National Laboratory for Information Science and Technology, Department of Electronic Engineering, Tsinghua University, Beijing 100084, China

(Received January 1, 2017; accepted March 16, 2017; published online April 11, 2017)

Backscattering in silicon micro-ring resonators is due to the side wall roughness of the waveguides, which leads to the backward coupling of light to the counter-propagating modes. In this paper, the impact of backscattering on the photon pair generation in a silicon micro-ring resonator with a quality factor (Q) of $\sim 10^4$ is investigated experimentally. It shows that due to the effect of backscattering, the two photons in a pair not only output from the resonator forwardly, but also both output backwardly, or even one forwardly and the other backwardly. Analysis on the coincident counts of different output port combinations shows that the effect of the pump light reflection due to the backscattering is weak. The reason for that the photon pairs output from all the port combinations is mainly due to the reflection of the generated signal/idler photons by the backscattering in the resonator. The experiments of Franson-type interference are taken to investigate the property of energy–time entanglement in the photon pairs outputting from different directions. The experiment results show that the backscattering may impact the interference fringes, however, energy–time entanglement exists in all the cases under our experiment condition.

1. Introduction

Silicon micro-ring resonators are important candidates to generate correlated photon pairs, which are widely used in the research of quantum computation, quantum communication, and quantum metrology.[1–4] The principle of the photon pair generation in silicon micro-ring resonators is spontaneous four wave mixing (SFWM).[5–7] The most widely used scheme uses a monochromatic continuous wave light as the pump light. It injects into the silicon micro-ring cavity at a specific resonance (with a frequency of ω_p). Two pump photons will be annihilated due to the SFWM, generating a pair of correlated photons at adjacent resonances simultaneously. The photon at higher resonance frequency (denoted by ω_s) is named signal and the one with lower resonance frequency (denoted by ω_i) is named idler. Their frequencies satisfy the relation of $\omega_s + \omega_i = 2\omega_p$, due to the energy conservation in the SFWM process. Thanks to the high nonlinearity of the silicon waveguides and the field enhancement at the resonances, photon pairs can be generated in silicon micro-ring resonators under low pump power. On the other hand, the spectrum of spontaneous Raman scattering in silicon waveguides is narrow and easy to be filtered out, hence, the noise performance of the photon pair generation by this way is excellent in room temperature.

Many works have been taken to demonstrate the performance of photon pair generation based on the silicon micro-ring resonators.[1–6] It was also shown that based on it, biphoton states with various entanglements could be realized with high performance.[8–14] Recently, some quantum interference experiments were realized on-chip by integrating the micro-ring resonators and interferometers together, showing its potential on photonic quantum circuits.[15] However, there are some non-ideal properties of the silicon micro-ring resonators which would impact the photon pair generation process, e.g., the backscattering. The backscattering widely exists in the whisper gallery mode type resonators.[16–24] In the silicon micro-ring resonators, the roughness of the side walls of the silicon waveguides would induce backward coupling to the counter-propagating modes. In a resonator with a high quality factor (Q), the backscattering may be too strong to be neglected.[23,24] It would impact both the pump light and the photons of the generated photon pairs, leading that the photon pairs are generated and extracted from the resonator in different directions. In this paper, this phenomenon is investigated experimentally for the first time.

2. Experiment about the Impact of Backscattering on Output Directions of Photon Pairs

2.1 *Experiment setup*

The silicon micro-ring resonator sample we used in the experiment has a resonator coupling with a bus waveguide. It is mounted on a manual alignment system and the light is coupled into and out of the bus waveguide by two lensed fibers. The micro-ring resonator has a perimeter of 132.5 μm. The width and height of its waveguide are 500 and 220 nm, respectively. At the ends of the bus waveguide, tapered structures are fabricated to extend the modal field and reduce the Fresnel reflection between the waveguide and air. The property of the sample is measured by a telecom band tunable laser (Santec TSL510) under an output power of 0 dBm. Only the quasi-TE mode of the waveguide is used in this experiment. Figure 1 shows the transmission spectrum, in which the dips in the spectrum show the resonances of the micro-ring resonator. It can be seen that the transmission spectrum is quite smooth at the off-resonance wavelength, which implies that the Fresnel reflection between the waveguide and the air is quite small thanks to the tapered structures. The sample has an insertion loss of 10 dB if the light is off-resonance. The resonances at 1556.03, 1547.06, and 1565.12 nm are used in the experiment for the pump light and generated signal/idler photons, respectively. By the transmission spectra shown in Fig. 1, the properties of the resonances used for the pump light and generated signal/idler photons in the experiment can be calculated, which are shown in Table I.

The experiment setup is shown in Fig. 2. The tunable laser is used as the continuous wave (CW) pump light source. It is tuned to 1556.03 nm, which is the wavelength of the resonance for the pump light. A set of tunable optical band-

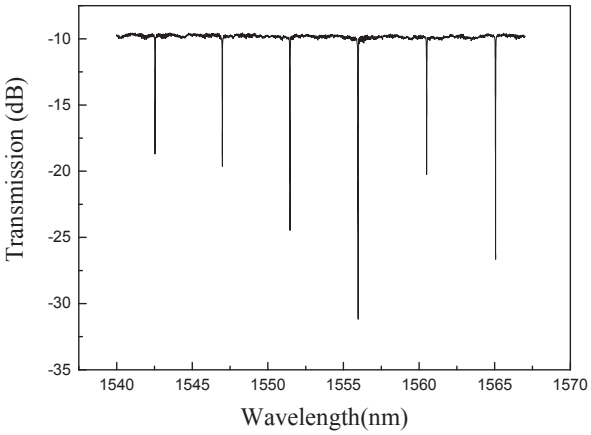

Fig. 1. The transmission spectrum of the micro-ring resonator sample measured by a tunable laser.

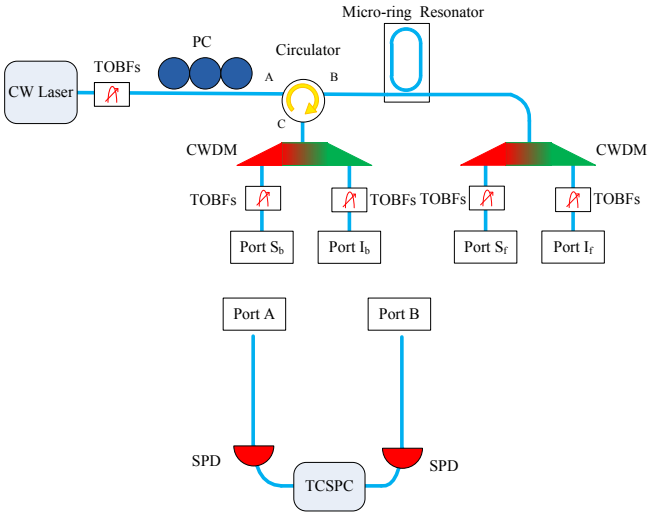

Fig. 2. (Color online) The experiment setup. CW laser: continuous wave laser. TOBF: tunable optical bandpass filter. PC: polarization controller. SPD: single photon detector. TCSPC: time-correlated single-photon counting. CWDM: coarse wavelength division multiplexer. Port A and Port B represent the output ports used for the coincident counting, including four combinations (Port S_f and Port I_f, Port S_b and Port I_b, Port S_f and Port I_b, Port S_b and Port I_f).

Table I. Parameters of the resonances for the pump light, signal photons and idler photons.

Resonances	Pump	Signal	Idler
Wavelength/nm	1556.03	1547.06	1565.12
3 dB linewidth/nm	0.03	0.025	0.035
Q factor	5×10^4	6×10^4	4×10^4
Extinction ratio/dB	21	10	17

pass filters (TOBFs) is used to suppress the noise photons at the resonance wavelengths for the signal and idler photons. Then the pump light is injected into the micro-ring resonator sample through a polarization controller (PC) and a circulator. The PC is used to ensure that the pump light propagate in the quasi-TE mode of the silicon waveguide. By the SFWM in the silicon micro-ring resonator, signal and idler photons are generated. Due to the backscattering, the generated photons output not only from the forward direction but also from the backward direction. In the forward direction, the signal and idler photons are separated by a coarse wavelength division multiplexer (CWMD) and selected by two sets of TOBFs at 1547.06 and 1565.12 nm, respectively. The forward output ports of the signal and idler photons are indicated by Port S_f and Port I_f, respectively. In the backward direction, the signal and idler photons pass through the circulator firstly, then selected by a CWDM and TOBFs similar with those in the forward direction. The backward output ports of the signal and idler photons are indicated by Port S_b and Port I_b, respectively. To demonstrate the impact of backscattering, the properties of photon pair generation under different output port combinations (Port S_f and Port I_f, Port S_b and Port I_b, Port S_f and Port I_b, Port S_b and Port I_f) are measured by two single photon detectors (SPDs; IDQ Id220) and a time-correlated single-photon counting equipment (TCSPC; Becker & Hickl DPC-230). The detection efficiencies of SPDs are set at 10% and the time bin width of the TCSPC is 164.6 ps.

2.2 *Experiment result*

Firstly, the effect of backscattering on the pump light is observed. The input power of the pump light is set as 1.5 dBm at Port A of the circulator. When the pump wavelength is tuned to be off-resonance, the pump light would not couple into the micro-ring resonator and pass through the bus waveguide directly. The measured power collected by the lensed fiber coupling to the output end of the bus waveguide is −8.5 dBm. The power of the backward pump light measured at Port C of circulator is −18.5 dBm, which is mainly due to the reflections introduced by the interfaces of the chip and the lensed fibers. When the pump wavelength is tuned to be on-resonance, the measured power at the output lensed fiber reduces to −31.0 dBm. While, the power of the backward pump light measured at Port C of the circulator increases to −8.2 dBm, which shows that most pump light is backscattered by the micro-ring resonator in this case. As a comparison, Ref. 19 investigated the back reflection of the silicon micro-ring resonator, showing that 31.6% (−5 dB) of the input power injected into a silicon micro-ring resonator with a coupling ratio of 0.2 could be reflected. Considering that Q value of the ring-resonator we used is much higher, the measured back reflection ratio when pump light is on resonance is reasonable.

Then, the single photon count rates at the four output ports are measured under different pump levels respectively. At each pump level, the pump wavelength needs to be adjusted to be on-resonance. The experiment results are shown in Fig. 3 by a log–log plot. In the figure, the pump power is measured at Port A of the circulator. The dark counts of the SPD are subtracted in all the results, which is 1 kHz. The error bars are calculated by the square roots of the single side counts. The black squares and red circles are results measured at Port S_f and Port I_f, respectively, which are two forward output ports. The black and red lines are their linear fitting lines in the log–log plot, with slopes of 1.90 and 1.89, respectively. The slopes are close to 2, showing that the recorded photons at the two forward ports are mainly due to the photon pairs generated by the SFWM in the micro-ring resonator, which rise in proportional to the square of the pump level. The blue and pink triangles are the results of Port S_b and Port I_b, respectively, which are two backward

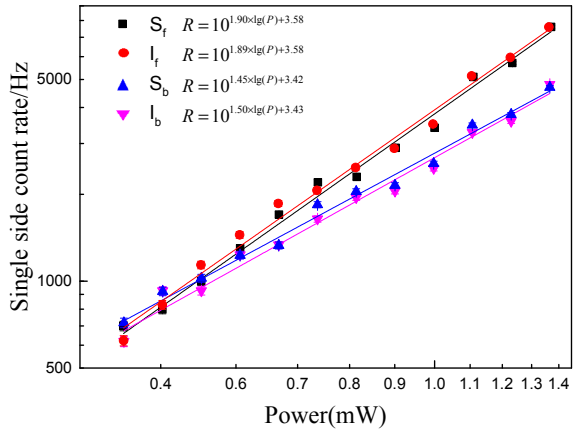

Fig. 3. (Color online) The experiment result of single side counting. The black squares, red circles, blue up-triangles, and pink down-triangles denote the experiment results measured at Port S_f, Port I_f, Port S_b, and Port I_b, respectively. The black line, red line, blue line, and pink line are their linear fitting lines, respectively. The fitting results are shown in the figure, in which R is the single side count rate and P is the pump power.

output ports. It can be seen that the photon count rates of the two backward ports are at the same level with those of the two forward ports. The blue and pink lines are their linear fitting lines in the log–log plot, with slopes of 1.45 and 1.50, respectively. The two slopes are both higher than 1, showing that the output photons from the two backward ports have contributions of the SFWM in the micro-ring resonator. However, they are both much lower than 2, showing that there are other noise photons outputting from the two backward ports. In the experiment of photon pair generation in silicon waveguides and resonators, usually two types of noise photons need to be considered. One is the photons generated by the spontaneous Raman scattering when the pump light propagates along the optical fibers in the experiment setup. To estimate its impact, we measured the Raman noise photons in the experiment setup by omitting the silicon chip, under the condition that the insertion loss of the fiber to fiber coupling is the same as that of the silicon chip by proper fiber alignment. When the input power of the pump light is set as 1.5 dBm at Port A of the circulator, the photon count rates at port S_f and I_f are both 0.35 kHz, far smaller than those shown in Fig. 3 (>5 kHz at 1.5 dBm), showing that the impact of spontaneous Raman scattering is not serious. The other is the residual pump photons due to the imperfect filtering. Since the two slopes for the two forward ports are both close to 2, the residual pump photons are also not serious for the two forward ports. However, the previous observation of the pump light shows that when the pump light is on-resonance, the pump light outputting backwardly from the sample is much higher than that outputting forwardly due to the backscattering in the micro-ring resonator. Hence, we can expect that the impact of the residual pump photons is much higher on the slopes for the two backward ports, which leads to their deviations from 2.

The results of the single side counts show that the photons outputting from the two backward ports also have the contribution of the SFWM in the micro-ring resonator. It can be expected that photon pairs not only output from the two forward ports (Port S_f/Port I_f), but also have the possibilities to output from other three output port combinations (Port S_f/Port I_b, Port S_b/Port I_f and Port S_b/Port I_b). To demonstrate the effect of the backscattering effect, we measure the coincident counts of above output port combinations under different pump levels. The power of the pump light is measured before Port A of the circulator, as well. The experiment results are shown in Fig. 4. Figure 4(a) shows a typical histogram of the coincident counting. The record time

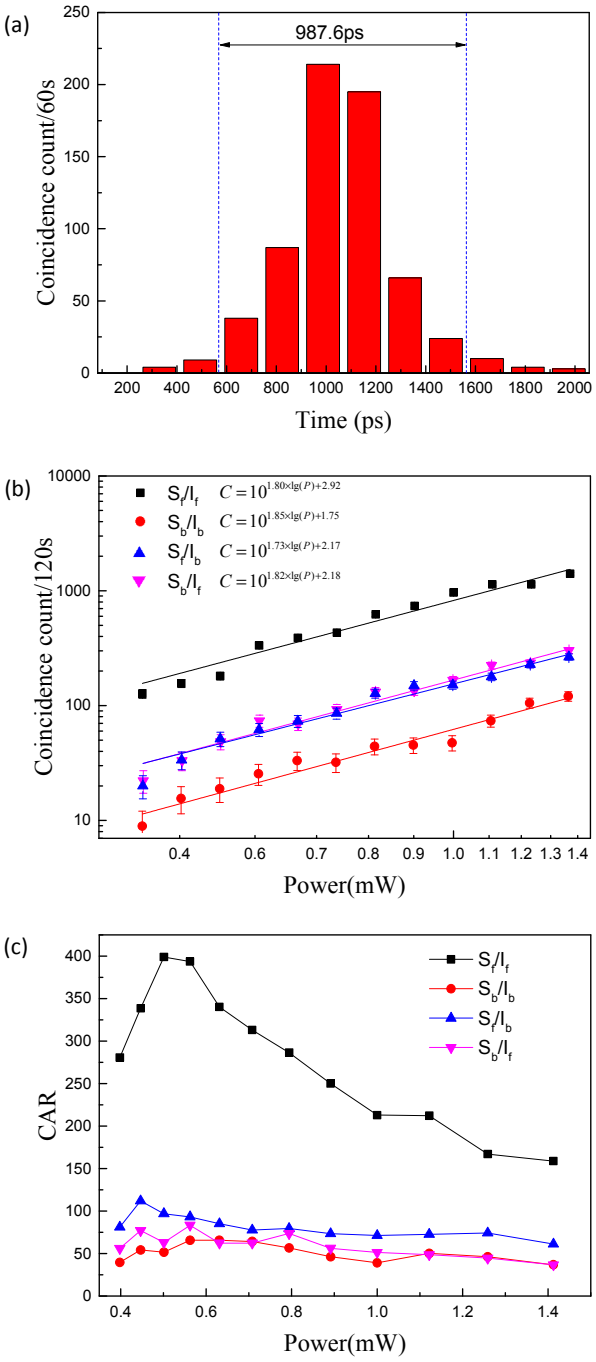

Fig. 4. (Color online) The experiment results of coincident counts of the four port combinations under different pump levels. (a) A typical histogram of the coincident counting. (b) The experiment result of coincident counts. The black squares, red circles, blue up-triangles, and pink down-triangles are the measured results of Port S_f/Port I_f, Port S_b/Port I_b, Port S_f/Port I_b, and Port S_b/Port I_f, respectively. Black, red, blue, and pink lines are their fitting lines, respectively. (c) The experiment results of CAR of the four port combinations. The black squares, red circles, blue up-triangles, and pink down-triangles are the results of Port S_f/Port I_f, Port S_b/Port I_b, Port S_f/Port I_b, and Port S_b/Port I_f, respectively.

is 120 s. The detection efficiencies of the SPDs are set at 10% and their time jitters are about 400 ps. The coincident counts are calculated by the sum of 6 time bins covering the coincidence peak, which is marked between the two blue lines in Fig. 4(a). The measured coincident counts of the four output port combinations are shown in Fig. 4(b). They are raw counts including the contributions of accidental coincident counts. The error bars are calculated by the square root of the results. The black squares, red circles, blue up triangles and pink down triangles are the results of Port S_f/Port I_f, Port S_b/Port I_b, Port S_f/Port I_b, and Port S_b/Port I_f, respectively. It can be seen that for all the output port combinations, there are obvious coincident counts recorded, which rise with increasing pump level. Among the four cases, the two forward ports (Port S_f/Port I_f) have the highest coincident counts under all the pump levels. The coincident counts of the two backward ports (Port S_b/Port I_b) are the smallest. The coincident counts of the two cases with one forward port and one backward port (Port S_f/Port I_b and Port S_b/Port I_f) are in the middle. The black, red, blue, and pink lines are their fitting lines with slopes of 1.80, 1.85, 1.73, and 1.82 in the log–log plot. All the slopes are all close to 2, showing that under all the port combinations the main contribution of the coincident counts is due to the photon pairs generated by the SFWM in the micro-ring resonator. Figure 4(c) shows the coincidence to accidental coincidence ratio (CAR) of the four port combinations under different pump levels. It can be seen that high CAR can be realized at all the port combinations. The highest CAR of Port S_f and I_f is about 400. Among the four port combination, Port S_b/I_b show the smallest CAR, which also can reach 65 under a proper pump level. Hence, although the raw data are used in the line fitting in Fig. 4(b), their small deviations from 2 could not be explained by the residual pump photons due to the imperfect filtering or dark counts of the SPDs. It should be due to the nonlinear loss in the micro-ring resonator, which would impact the photon pair generation rate at high pump level.[2,4,6)]

It is obvious that the strong backscattering in the micro-ring resonator is the reason for that the photon pairs output from all the port combinations. Specifically, it may lead to two possible effects. On one hand, the pump light may be reflected by the backscattering in the resonator, generating photon pairs backwardly. Here, we define a parameter p to represent the possibility that a measured photon pair is generated by the forward pump light in the resonator. Hence, $1-p$ is the possibility that it is generated by the backward pump light due to the backscattering. On the other hand, the generated signal and idler photons also can be reflected by the backscattering. We define a parameter r to represent the possibility that a generated signal/idler photon is reflected by the backscattering in the resonator then output from the resonator. Hence, $1-r$ is the possibility that the generated photon is not reflected before it outputs from the resonator. Assuming that the photon pair generation rate is R and the collection efficiencies of the four ports are the same, which is denoted by η, the coincident count rates of the four port combination can be expressed as

$$N(S_f, I_f) = R\eta^2[p(1-r)^2 + (1-p)r^2], \quad (1)$$

$$N(S_b, I_b) = R\eta^2[pr^2 + (1-p)(1-r)^2], \quad (2)$$

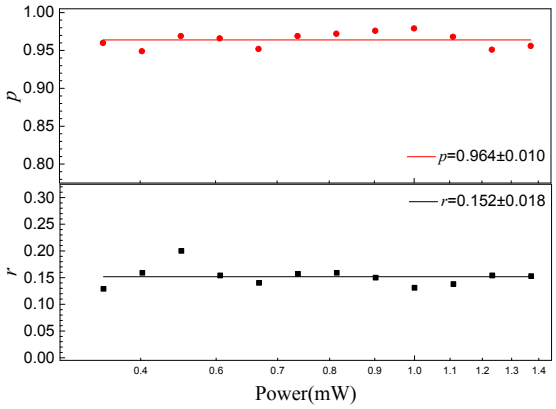

Fig. 5. (Color online) The calculated p and r under different pump levels.

$$\begin{aligned} N(S_f, I_b) &= N(S_b, I_f) \\ &= R\eta^2[pr(1-r) + (1-p)(1-r)r] \\ &= R\eta^2(1-r)r, \end{aligned} \quad (3)$$

where $N(S_f, I_f)$, $N(S_b, I_b)$, $N(S_f, I_b)$, and $N(S_b, I_f)$ are the coincident count rates of the four port combinations. If the sum of them is denoted by S, it is easy to conclude that $S = N(S_f, I_f) + N(S_b, I_b) + N(S_f, I_b) + N(S_b, I_f) = R\eta^2$. It can be seen that

$$N(S_f, I_f)/S = p(1-r)^2 + (1-p)r^2, \quad (4)$$

$$N(S_b, I_b)/S = pr^2 + (1-p)(1-r)^2, \quad (5)$$

$$N(S_f, I_b)/S = (1-r)r. \quad (6)$$

Using the experiment results shown in Fig. 4(b), the lefts of Eqs. (4)–(6) can be calculated under different pump levels, then p and r in the micro-ring resonator used in this experiment are calculated and shown in Fig. 5. It can be seen that the calculated p and r under different pump levels agree well. The average p is 96.4%, it means that almost all the pairs are generated forwardly in the resonator. The effect of the pump light reflection due to the backscattering is weak. Hence, the reason for that the photon pairs output from all the port combinations is mainly due to the reflection of the generated signal/idler photons, which has a possibility of 15.2% (estimated by the average r) to be reflected by the backscattering in the resonator.

3. Experiment about the Impact of Backscattering on Energy–Time Entanglement of Photon Pairs

3.1 Experiment setup

It is well known that the generated photon pairs have the property of energy–time entanglement intrinsically if a monochromatic CW pump light is used to stimulate the SFWM in the resonator.[8–11,14)] An interesting question is whether the backscattering effect on the signal and idler photons in a pair impacts its energy–time entanglement. In this work, we took experiments of Franson-type interference under all the four output port combinations. The setup for the Franson-type interference is shown in Fig. 6(a). The power of the pump light is 1.5 dBm, which is measured before Port A of the circulator. The photons output from two specific ports would pass through unbalanced Mach–Zander interferometers (UMZIs; Kylia mint-1×2-L-2.5GHz) firstly. Then they are detected by the two SPDs. For each UMZI, the arm difference is 400 ps, and the phase difference between the

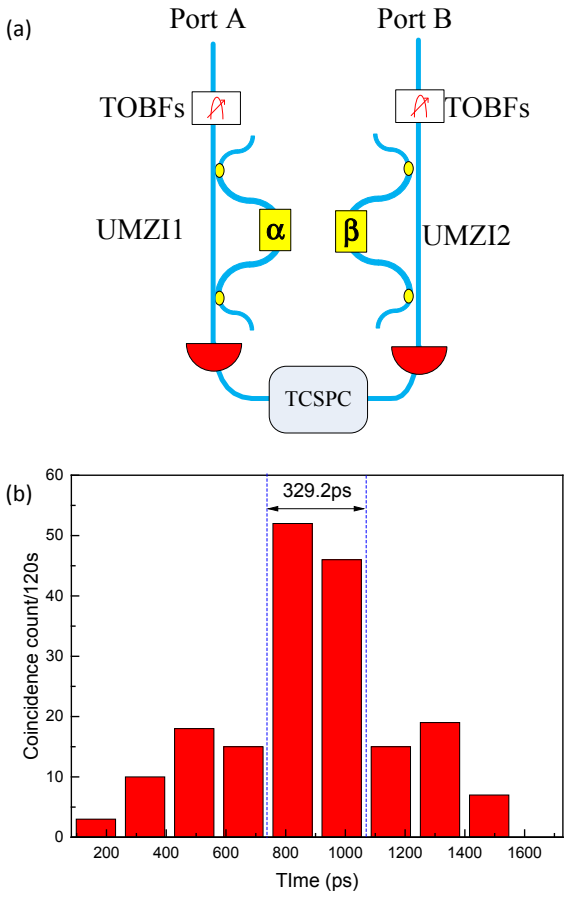

Fig. 6. (Color online) Setup for the Franson-type interference. (a) The experiment setup. UMZI: unbalanced Mach–Zander interferometer. (b) A typical histogram of the coincidence measurement.

long arm and the short arm is tunable. The phase differences between the two arms of the two UMZIs are denoted by α and β, respectively. If the time difference of the two arms is longer than the coherence time of the signal and idler photons, but much shorter than the coherent time of the two photon wave packet, energy–time entanglement could be demonstrated by the Franson-type interference. In this experiment, the counting time is 60 or 120 s according to the ports in the measurement. The detection efficiencies of the two SPDs are set to 20% in order to reduce their time jitters to 250 ps, by which the width of the coincidence peaks are also reduced and the three coincidence peaks can be discriminated. The coincident counts are calculated by the sum of two time bins covering the coincidence peak, which is marked between the two blue lines in Fig. 6(b). Figure 6(b) shows a typical raw coincidence when the setup connects to Port S_f and Port I_b. Each bar in the histogram shows the coincident counts in a specific time bin. It can be seen that there are three peaks in the histogram. The left and right peaks are the contributions that one photon of the pair propagates through the long arm of a UMZI, while the other propagates through the short arm of the other UMZI. The central peak is the contribution that the signal and idler photons in a pair either both propagate through the long arms of the two UMZIs or both propagate through the short arms of the two UMZIs. The two cases are indistinguishable in the coincident counting and have equal possibilities, leading to a quantum interference. The interference is determined by the phase differences of the two UMZIs (α and β). If β is fixed and the coincident count is measured under different α, the central peak would vary with α, showing a sinusoidal interference fringe. If photon pairs have the property of energy–time entanglement, the fringe would show high visibility (>70.7%, the benchmark for violation of Bell inequality[9–11]) under all the β. Usually, the measurements of the Franson-type interference under two nonorthogonal phase bases are used to demonstrate the energy–time entanglement.

3.2 *Experiment result*

Figure 7 is the measured Franson-type interference fringes at different output port combinations. Raw data with the contribution of accidental coincident counts are shown in Fig. 7. The error bars are calculated by the square root of the data. Here, the counts of the central peak are calculated by the sum of the two time bins covering the central peak, which is shown between the two blue dot lines in Fig. 6(b). In each figure, two fringes are measured under two different β. Their values are selected that their difference is not equal to the integer multiple of $\pi/2$, hence, two nonorthogonal bases are used. Figures 7(a), 7(b), 7(c), and 7(d) show the results of the four output port combinations (Port S_f/Port I_f, Port S_f/Port I_b, Port S_b/Port I_f, and Port S_b/Port I_b) respectively. The visibilities of measured fringes at different output port combinations are summarized at Table II. It can be seen that for the two forward output ports (Port S_f/Port I_f), the visibilities of the two fringes are $93.7 \pm 3.0\%$ and $97.9 \pm 1.4\%$ when $\beta = 3.34$ and 3.91, respectively. Both of them are far higher than 70.7%. For other output port combinations, the fringe visibilities reduce, however, they are still higher than 70.7%. The single side counts of signal and idler photon do not change when α varies under a fixed β for all the combinations of ports. The difference between the amplitudes of the two fringes in a figure is due to that the alignment between the micro-ring resonator sample and lensed fibers drifts slowly during the measurement and sometimes re-alignment is required.

The experiment results in Table II shows that the fringe visibilities of the two forward ports is quite high, however, those of the other three port combinations are obviously lower, although energy–time entanglement still can be demonstrated. It can be explained by the analysis in previous section. It shows that in the resonator, most photon pairs generated forwardly, while, parts of signal and idler photons are reflected by the backscattering, leading that photon pairs may output from all the port combination. For the photon pairs outputting from the two forward output ports, both the signal and the idler photons are not reflected. The back-scattering does not impact the fringe visibilities of the Franson-type interference. However, for the photon pairs outputting from the other three port combinations, at least one photon in a pair is reflected. Since it might be reflected at any position in the resonator, it can be expected that the reflection would impact the coherence of the two-photon wavepacket of the photon pair. This effect would reduce the fringe visibilities of the Franson-type interference.

4. Conclusion

In conclusion, we have investigated the impact of back-

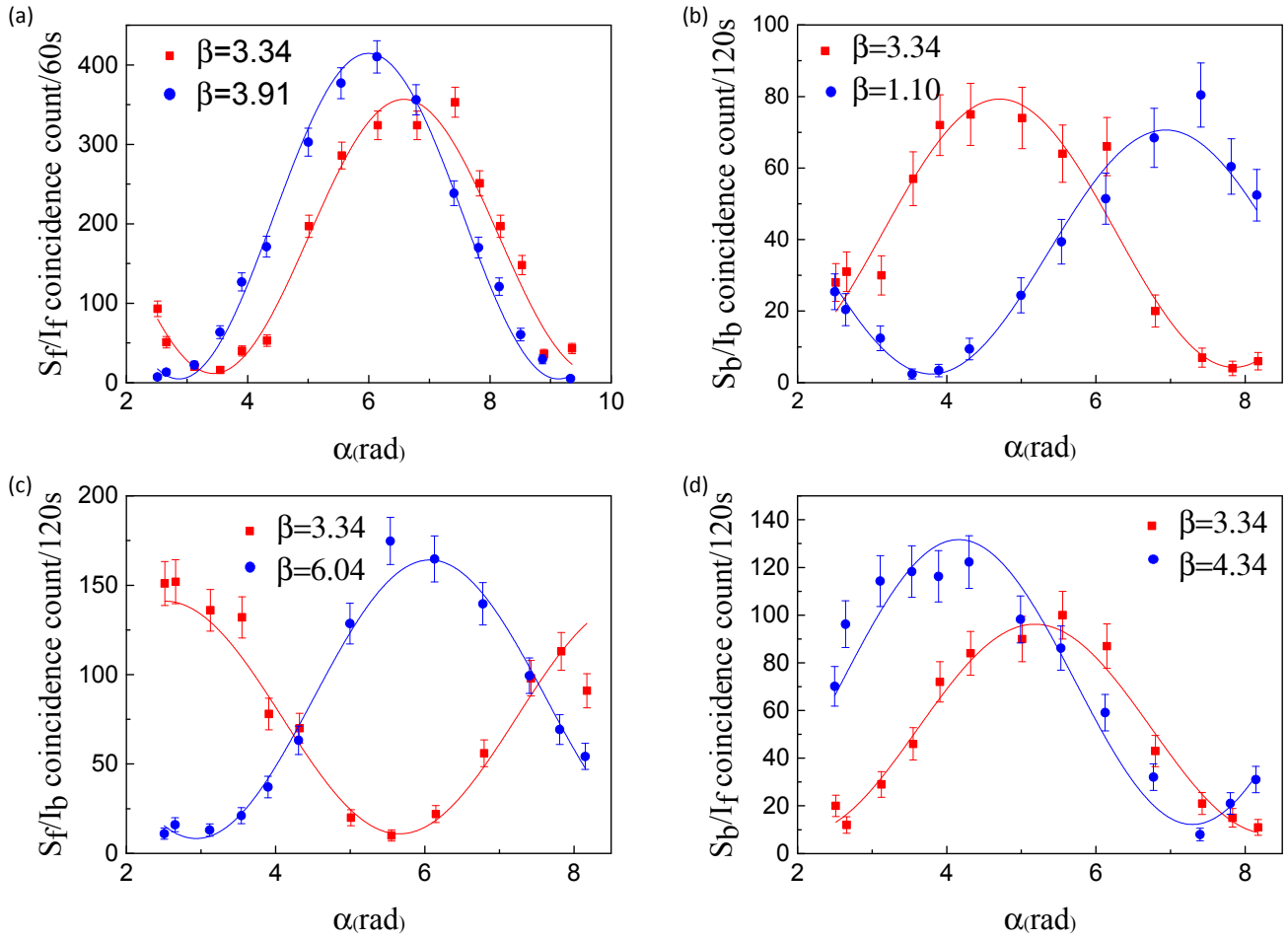

Fig. 7. (Color online) The experiment results of the Franson type interferences under four output port combinations. (a) Coincident counts of Port S_f/Port I_f within 60 s. (b) Coincident counts of Port S_b/Port I_b within 120 s. (c) Coincident counts of Port S_f/Port I_b within 120 s. (d) Coincident counts of Port S_b/Port I_f within 120 s.

Table II. The visibilities of measured fringes at different output port combinations.

	Port S_f/Port I_f	Port S_f/Port I_b	Port S_b/Port I_f	Port S_b/Port I_b
Visibility of red fringe	$\beta = 3.34$ $v = 93.7 \pm 3.0\%$	$\beta = 3.34$ $v = 89.7 \pm 3.8\%$	$\beta = 3.34$ $v = 85.6 \pm 4.9\%$	$\beta = 3.34$ $v = 84.1 \pm 3.5\%$
Visibility of blue fringe	$\beta = 3.91$ $v = 97.9 \pm 1.4\%$	$\beta = 1.10$ $v = 94.4 \pm 2.4\%$	$\beta = 6.04$ $v = 91.4 \pm 2.2\%$	$\beta = 4.34$ $v = 84.2 \pm 4.1\%$

scattering on the photon pair generation in a silicon micro-ring resonator with a Q value of $\sim 10^4$ in this paper. It shows that due to the effect of backscattering, the two photons in a pair not only output from the resonator forwardly, but also may both output backwardly, or even one forwardly and the other backwardly. The analysis on the coincident counts of different output port combinations shows that the effect of the pump light reflection due to the backscattering is weak. The reason for that the photon pairs output from all the port combinations is mainly due to the reflection of the generated signal/idler photons, which has a possibility of 15.2% to be reflected by the backscattering in the resonator. In all these cases, the property of energy–time entanglement is demonstrated by the experiments of Franson-type interference. It shows that the backscattering may impact the interference fringes, however, energy–time entanglement exists in all the cases under our experiment condition.

Acknowledgments

This work was supported by the National Natural Science Foundation of China under Contract Nos. 61575102 and 91121022, the 973 Programs of China under Contract Nos. 2013CB328700 and 2011CBA00303; the Tsinghua University Initiative Scientific Research Program under Contract No. 20131089382; and the Tsinghua National Laboratory for Information Science and Technology.

*zwei@tsinghua.edu.cn

1) S. Clemmen, K. P. Huy, W. Bogaerts, R. G. Baets, P. Emplit, and S. Massar, Opt. Express **17**, 16558 (2009).
2) S. Azzini, D. Grassani, M. J. Strain, M. Sorel, L. G. Helt, J. E. Sipe, M. Liscidini, M. Galli, and D. Bajoni, Opt. Express **20**, 23100 (2012).
3) E. Engin, D. Bonneau, C. M. Natarajan, A. Clark, M. G. Tanner, R. H.

Hadfield, S. N. Dorenbos, V. Zwiller, K. Ohira, N. Suzuki, H. Yoshida, N. Iizuka, M. Ezaki, J. L. O'Brien, and M. G. Thompson, Opt. Express **21**, 27826 (2013).
4) Y. Guo, W. Zhang, N. Lv, Q. Zhou, Y. Huang, and J. Peng, Opt. Express **22**, 2620 (2014).
5) L. G. Helt, Z. Yang, M. Liscidini, and J. E. Sipe, Opt. Lett. **35**, 3006 (2010).
6) S. Azzini, D. Grassani, M. Galli, L. C. Andreani, M. Sorel, M. J. Strain, L. G. Helt, J. E. Sipe, M. Liscidini, and D. Bajoni, Opt. Lett. **37**, 3807 (2012).
7) B. Fang, O. Cohen, J. B. Moreno, and V. O. Lorenz, Opt. Express **21**, 2707 (2013).
8) J. Suo, S. Dong, W. Zhang, Y. Huang, and J. Peng, Opt. Express **23**, 3985 (2015).
9) D. Grassani, S. Azzini, M. Liscidini, M. Galli, M. J. Strain, M. Sorel, J. E. Sipe, and D. Bajoni, Optica **2**, 88 (2015).
10) R. Kumar, M. Savanier, J. R. Ong, and S. Mookherjea, Opt. Express **23**, 19318 (2015).
11) R. Wakabayashi, M. Fujiwara, K. Yoshino, Y. Nambu, M. Sasaki, and T. Aoki, Opt. Express **23**, 1103 (2015).
12) J. W. Silverstone, R. Santagati, D. Bonneau, M. J. Strain, M. Sorel, J. L. O'Brien, and M. G. Thompson, Nat. Commun. **6**, 7948 (2015).
13) J. He, B. A. Bell, A. Casas-Bedoya, Y. Zhang, A. S. Clark, C. Xiong, and B. J. Eggleton, Optica **2**, 779 (2015).
14) J. Suo, W. Zhang, S. Dong, Y. Huang, and J. Peng, J. Phys. Soc. Jpn. **85**, 104401 (2016).
15) N. C. Harris, D. Grassani, A. Simbula, M. Pant, M. Galli, T. Baehr-Jones, M. Hochberg, D. Englund, D. Bajoni, and C. Galland, Phys. Rev. X **4**, 041047 (2014).
16) F. Ladouceur and L. Poladian, Opt. Lett. **21**, 1833 (1996).
17) F. Morichetti, A. Canciamilla, C. Ferrari, M. Torregiani, A. Melloni, and M. Martinelli, Phys. Rev. Lett. **104**, 033902 (2010).
18) F. Morichetti, A. Canciamilla, and A. Melloni, Opt. Lett. **35**, 1777 (2010).
19) F. Morichetti, A. Canciamilla, M. Martinelli, A. Samarelli, R. M. De La Rue, M. Sorel, and A. Melloni, Appl. Phys. Lett. **96**, 081112 (2010).
20) B. E. Little, J. Laine, and S. T. Chu, Opt. Lett. **22**, 4 (1997).
21) W. C. Jiang, X. Lu, J. Zhang, O. Painter, and Q. Lin, Opt. Express **23**, 20884 (2015).
22) G. C. Ballesteros, J. Matres, J. Martí, and C. J. Oton, Opt. Express **19**, 24980 (2011).
23) M. Borselli, T. J. Johnson, and O. Painter, Opt. Express **13**, 1515 (2005).
24) T. J. Kippenberg, S. M. Spillane, and K. J. Vahala, Opt. Lett. **27**, 1669 (2002).